Jurnal MIPA dan Pembelajarannya
e-issn: 2798-0634, email: jmipap.journal@um.ac.id

VOL	ISS	YEAR	DOI
6	7	2026	10.17977/um067.v6.i7.2026.4

INCREASING THE INFLUENCE OF POLYMERS IN LITHIUM BATTERIES

Fahmi Yekti Waluyo[1], Markus Diantoro[1,2*]

[1] Departemen Fisika, Fakultas Matematika dan Ilmu Pengetahuan Alam, Universitas Negeri Malang, Malang, Indonesia, 65145

[2] Center of Advanced Material for Renewable Energy, Universitas Negeri Malang, Malang, Indonesia, 65145*

Corresponding author, email: markus.diantoro.fmipa@um.ac.id

Keywords
Polymer
Battery
Lithium

Abstract
Recently, there has been much innovation in the energy storage system. The famous energy storage system now is Lithium battery, due to high energy density, little capacitance lost, and efficiency. But in the way of explosion, extreme temperature, liability to explode again, and precipitate lithium that didn't evenly become bad for lithium batteries. Actually, now there is much research innovation to enhance lithium batteries performance. Mostly in modification materials like synthesis, doped, and composite. And in another way, polymers also turn out to be material batteries. In 1970 some scientists discovered an innovative polymer for battery material. It's an open new view in science knowledge, especially material development of batteries. Therefore, these research polymers in lithium batteries material to increase. To responses of enhancement performance of lithium batteries material, we make comparison between polymer usage and non-polymer usage (synthesis, doped, composite) for lithium batteries. The result from non-polymer usage showed composite had highest specific capacity (1349 mAh.g-1), but doped also had high specific capacity even though not more than composite methods. On the other hand, the use of polymers showed the highest specific capacity of 2237 mAh.g-1. However, the use of non-polymers was far superior, providing higher average specific capacity values. Therefore, the use of common materials modified through synthesis, doping, and composites remains the best way to improve the performance of lithium batteries today.

1. Introduction

The increase in industrialization is directly proportional to the growing energy demand but inversely proportional to the availability of fossil fuels. Combined with population growth, this has accelerated the adoption of renewable energy technologies (Awan et al., 2024). Furthermore, the depletion of non-renewable fossil fuel resources has led to the increasing prominence of renewable energy storage systems, particularly lithium-ion batteries (LIBs), which have dominated the market over the past three decades (Li et al., 2026). Their advantages, including high energy density, low capacity loss, and high efficiency, have further strengthened their position in modern energy storage applications (Marco et al., 2026). As a result, lithium-ion batteries (LIBs) have become increasingly prevalent in contemporary society.

However, throughout their development, numerous fire incidents have been reported. According to the International Association of Fire and Rescue Services (CTIF), approximately three million fire incidents occurred across 46 countries in 2023, partly due to large-scale battery fires, extreme temperatures, and the tendency of batteries to reignite after extinguishment (Zhang et al., 2026). In addition, non-uniform lithium deposition on the anode can induce dendrite formation, electrolyte consumption, and active lithium loss, all of which negatively affect battery cycling performance (Ge et al., 2026). These challenges have encouraged the incorporation of additional materials, such as TiO_2 doping in Li–S batteries to address sluggish redox kinetics, suppress lithium dendrite growth, and enhance safety (Pang et al., 2026). Similarly, graphene-based FeS_2@NSC core–

shell composites have been employed to mitigate volume expansion, which is a major cause of structural degradation in Li–S batteries (Tu & Cao, 2026).

2. Literature Review

The discovery of conductive polymers in the late 1970s transformed the paradigm of materials science. Conductive polymers such as trans-polyacetylene (trans-PAc) exhibited electrical conductivity up to ten million times higher than conventional polymers while demonstrating reversible charge-storage capability. This breakthrough subsequently led to the development of conductive polymers including poly(phenylene) (PPh), polyaniline (PANI), polypyrrole (PPy), polythiophene (PTh), and poly(3,4-ethylenedioxythiophene) (PEDOT), among others (Singh & Jadoun, 2026). Moreover, polymers possess unique redox activity, efficient charge-transport properties, and readily tunable molecular structures, making them a major focus of contemporary research (Cui et al., 2026).

In battery technology, polymers have also emerged as promising solutions to address several limitations of conventional batteries. For example, gel polymer electrolytes (GPEs) have been utilized as electrolytes to provide enhanced safety and cycling stability in high-voltage lithium–oxygen batteries (LOBs) (Gong et al., 2026).

To date, research on polymers in lithium batteries has focused on several key areas. These include investigations into the evolution of gel polymer electrolytes (GPEs) and natural–synthetic hybrid systems for designing hybrid GPEs through blending, core–shell structures, and crosslinking strategies (Qayyum et al., 2026). Other studies have examined polymer electrolytes for silicon-anode lithium-ion batteries, including silicon-anode engineering approaches and compatibility assessments with oxide- and sulfide-based solid-state electrolytes (SSEs) (Rangasamy et al., 2026). Research has also explored pairwise interactions, interfacial failure mechanisms, and novel designs of conductive polymer electrodes and SSEs to develop safe, high-performance, and durable all-solid-state metal-ion batteries (Pandit et al., 2026). Furthermore, in situ radical polymerization has been analyzed with emphasis on initiation chemistry, formulation design, process control, mechanistic characteristics, practical advantages, and associated limitations (Luo et al., 2026).

Additional studies have investigated polymer binders for all-solid-state lithium batteries (ASSLBs), focusing on process compatibility and structural control to establish continuous ion-conduction pathways within electrode sheets and electrolytes (Hong et al., 2025). Research has also addressed interface science, polymer electrolyte (PE) engineering strategies, advanced PE designs, and the identification of challenges associated with polymer electrolytes in lithium-ion batteries (LIBs) (Hu et al., 2026). Moreover, ion-conduction mechanisms, including ion hopping in solid polymer electrolytes (SPEs), solvent-assisted transport in GPEs, polymer interfacial conduction in composite polymer electrolytes (CPEs), optimization strategies such as copolymerization and plasticization, single-ion conductors, artificial solid electrolyte interphase (SEI) layers, three-dimensional filler networks, interfacial contact challenges, cycling stability, manufacturing processes, future polymer-matrix developments, multiscale simulations, and flexible battery integration have been comprehensively examined (Liang et al., 2026). Advanced polymer topologies and architectures have also been investigated to balance conductivity, mechanical properties, and stability while enhancing functional performance. In situ and operando characterization techniques have been proposed to accelerate the rational design of solid-state polymer electrolytes (SSPEs) (Lan et al., 2026). Finally, corrosion phenomena in lithium-ion and sodium-ion batteries, together with the exploration of conductive polymer materials, have been systematically reviewed (Mohammadipour & Gharahcheshmeh, 2025).

Based on the findings of these literature studies, the development of polymers for lithium batteries

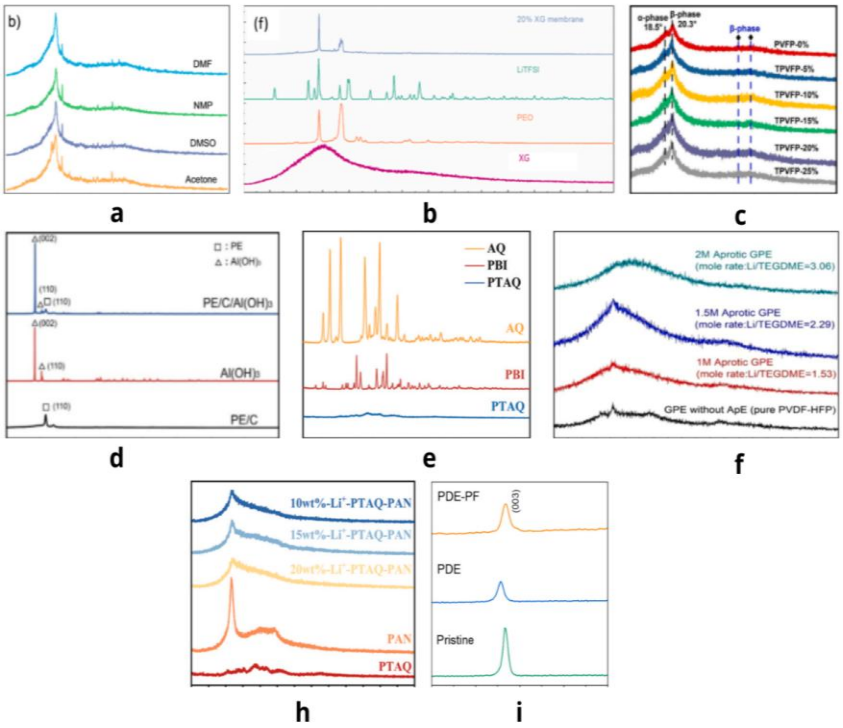

Figure 1. XRD data of [a] SPEs (Pinto et al., 2026), [b–c] PVFP and TPVFP (Hu et al., 2026), [d] PE/C/Al(OH)$_3$ (Wan et al., 2026), [e] LIPTAQ (Kong et al., 2026), [f] GPEs (Sabir et al., 2026), [g] LiPTAQ-PAN (Kong et al., 2026), and [h] PDE-PF (Ren et al., 2026).

have encompassed polymer electrolytes, interfacial anode optimization, all-solid-state lithium batteries (ASSLBs), synthesis methods, fabrication techniques, characterization results, and the exploration of novel materials. However, these studies have not yet clearly elucidated the extent to which polymer-based materials improve battery performance compared with lithium batteries employing alternative synthesized, doped, or composite materials. Therefore, a comprehensive analysis is required to compare the performance of lithium batteries with and without polymer-based materials.

3. Discusion

3.1. Use of Polymers in Lithium Batteries

3.1.1. XRD (X-Ray Diffraction)

The XRD patterns of various polymer materials used in lithium batteries exhibit characteristic features ranging from semi-crystalline to amorphous structures. Most samples display broad diffraction peaks within specific 2θ ranges, indicating the predominance of amorphous phases in the polymer matrix. In Figure 2(a), the use of acetone, DMSO, NMP, and DMF results in variations in diffraction peak intensity and sharpness, suggesting that the solvent type influences the degree of crystallinity and polymer-chain arrangement during membrane formation. In Figure 2(b), the XRD patterns of XG, PEO, and LiTFSI indicate that after composite membrane fabrication, several crystalline peaks decrease in intensity or disappear entirely. The data presented in Figure 2(c) reveal phase transitions between the α and β phases in PVDF-based polymer electrolytes with varying additive compositions. The shift and enhancement of β-phase peak intensity suggest that the incorporation of fillers or additives promotes the formation of the electroactive β-PVDF phase.

In Figure 2(d), the presence of characteristic peaks corresponding to Al(OH)$_3$ and PE/C confirms the successful formation of the composite material without disrupting the fundamental structures of the individual components. Figure 2(e) demonstrates differences in crystallinity among AQ, PBI, and PTAQ. AQ exhibits numerous sharp peaks, indicating a highly crystalline structure, whereas PTAQ displays broader diffraction features, reflecting a more amorphous nature. In Figure 2(f), increasing the LiTFSI/DEGDME ratio in the gel polymer electrolyte leads to broader diffraction peaks, indicating an increase in the amorphous phase due to interactions among the lithium salt, solvent, and PVDF-HFP matrix. Meanwhile, in Figures 2(h) and 2(i), the incorporation of fillers and polymer

modifications results in reduced intensity of the primary crystalline peaks and broadening of the diffraction patterns.

Overall, these XRD data demonstrate that polymer composition modification, filler incorporation, lithium-salt addition, and solvent variation significantly influence the crystallinity of the materials. Most modifications lead to reduced crystallinity and an increased amorphous phase fraction.

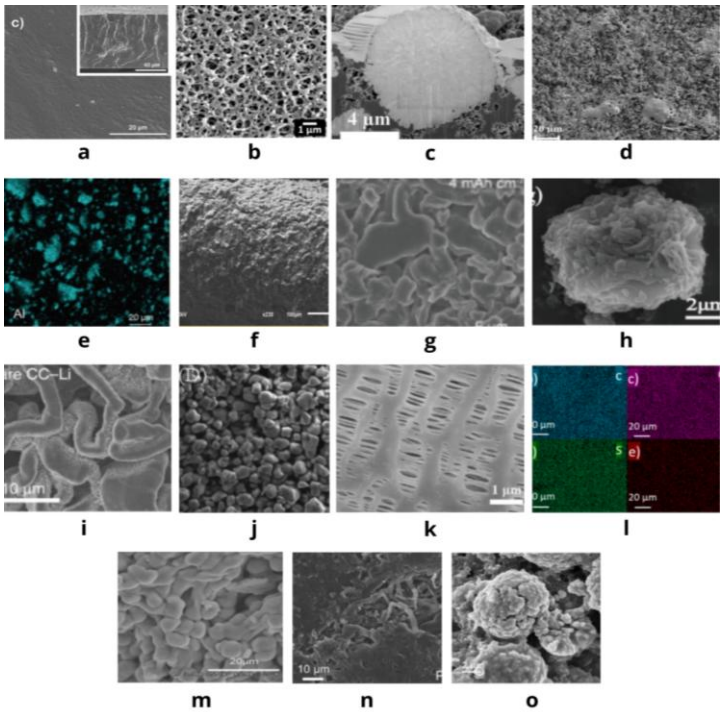

Figure 2. Morphology of [a] SPEs (Pinto et al., 2026), [b] PA+PES (Wang et al., 2026), [c] semi-IPN PEO-based SPEs (Nguyen et al., 2025), [d] Li|PL-PF-PL|$LiFePO_4$ (Feng et al., 2026), [e] PE/C/$Al(OH)_3$ (Wan et al., 2026), [f] CSF_2 (Muhainia et al., 2026), [g] PE/C/$Al(OH)_3$ (Wan et al., 2026), [h] LIPTAQ (Kong et al., 2026), [i] CO-Li, [j] $LiNbO_3$+$LiCoO_2$ (Thompson et al., 2025), [k] FGPE (Ge et al., 2026), [l] CoTP@CC–Li (Kim et al., 2026), [m] GPE (Sabir et al., 2026), [n] PDE-PF (Ren et al., 2026), and [o] Li||NCM811 (Chen et al., 2026).

According to Weckelmann et al. (2025), crystal structure plays a critical role in determining ionic conductivity because it directly influences the energy barrier associated with ion hopping. Structures such as body-centered cubic (bcc) lattices can enhance conductivity due to their relatively low hopping barriers. In general, polymers exhibit low conductivity at room temperature; therefore, conductivity enhancement requires structural engineering approaches, including the addition of lithium salts, plasticizers, and elevated operating temperatures.

Table 1. Relationship Between Polymer Utilization and Morphological Characteristics of Lithium Battery Materials

Polymer Material	Crystallite Size (nm)	Surface Area (m^2 g^{-1})	Reference
solid polymer electrolytes (SPEs)	-	-	Pinto et al., 2026
PE/C/$Al(OH)_3$	-	-	Wan et al., 2026
poly (acrylic acid)-polyamide (PA) + (PES)	-	-	Wang et al., 2026
CS, PVDF, CSF2	-	-	Mahaninia et al., 2026
PEO/ LiTFSI (EO/Li 1:21)	-	-	Patriarchi et al., 2026
CoTP@CC–Li	-	-	Kim et al., 2026
LiNbO3 coated LiCoO2 +Li Polymer	247 - 428	-	Thompson et al., 2025
semi-IPN PEO-based SPEs	-	-	Nguyen et al., 2025
FGPE	-	-	Ge et al., 2026
Li||NCM811	-	-	Chen et al., 2026
Li|PL-PF-PL|LiFePO4	-	-	Feng et al., 2026
PDE-PF	-	-	Ren et al., 2026
GPE	-	-	Sabir et al., 2026
PVFP dan TPVFP	-	-	Hu et al., 2026
LiPTAQ	-	265.64	Kong et al., 2026

3.1.2. Morphology

According to Chi et al. (2026), the use of polymers such as poly(ethylene oxide) (PEO) facilitates the breaking and reformation of coordination bonds between the polymer chains and Li^+ ions, thereby providing free volume for rapid Li^+ transport. This process occurs through a "decoordination–recoordination" mechanism that enables efficient ionic migration. Furthermore, Pandit et al. (2026) reported that smaller particle sizes increase the surface area of solid-state electrolyte (SSE) electrodes and additives, thereby enhancing mechanical stability. In addition, well-controlled morphologies can provide efficient ion-transport pathways, improve interfacial contact, and maintain a balance between material density and ionic conductivity.

As illustrated in Figure 2, polymer-based materials exhibit diverse surface morphologies, including smooth, porous, granular, and layered structures. Modifications in material composition also result in rougher and more irregular morphologies, indicating interactions among the components within the polymer matrix. As previously discussed, crystallite size plays an important role in determining mechanical stability. Based on the data presented in Table 1, the reported crystallite sizes (247–428 nm) are generally larger than those presented in Table 4. This suggests that the surface area and mechanical stability of non-polymer materials remain superior.

However, Weckelmann et al. (2025) noted that although crystalline phases were initially considered the primary ionic conductors, subsequent studies revealed that amorphous structures are, in most cases, the dominant pathways for ion transport, with the exception of PEO_6:$LiSbF_6$. Therefore, the predominantly amorphous structures observed in Figure 1 indicate potentially more effective ion-conduction behavior than the predominantly crystalline structures found in non-polymer materials. Consequently, the morphological data suggest that polymer materials possess both distinct advantages and inherent limitations when evaluated from a morphological perspective.

3.1.3. Electrochemical Impedance Spectroscopy (EIS)

Electrochemical Impedance Spectroscopy (EIS) is widely employed to evaluate ionic conductivity and the effects of fillers, synthesized materials, and composite structures. In Nyquist plots, the high-frequency region is typically represented by a semicircular arc corresponding to charge-transfer resistance at the electrode–electrolyte interface, whereas the low-frequency region is represented by an inclined line associated with ion-diffusion resistance within the electrode (Pandurangan et al., 2026).

The EIS results indicate that all samples exhibit semicircular behavior in the high- to intermediate-frequency regions, followed by a linear response at low frequencies. A smaller semicircle diameter corresponds to lower charge-transfer resistance, resulting in more efficient ion transport. Several samples also demonstrate reduced impedance following material modification or electrochemical cycling, indicating improvements in ionic conductivity and electrochemical stability. Furthermore, changes in the shape of the impedance curves after cycling suggest interactions between the electrolyte and electrode during battery charging and discharging processes.

3.1.4. Cyclic Voltammetry (CV)

As shown in Figure 4, the cyclic voltammetry (CV) results reveal distinct oxidation and reduction peaks, confirming the occurrence of redox reactions within the materials. The close overlap of CV curves over multiple cycles indicates good electrochemical reversibility and material stability during cycling. In addition, increases or shifts in peak current observed in several samples suggest that material modifications can significantly influence ion- and electron-transport kinetics.

The preservation of the CV curve profile in subsequent cycles further indicates that the materials exhibit satisfactory electrochemical performance, highlighting their potential suitability for lithium-battery applications.

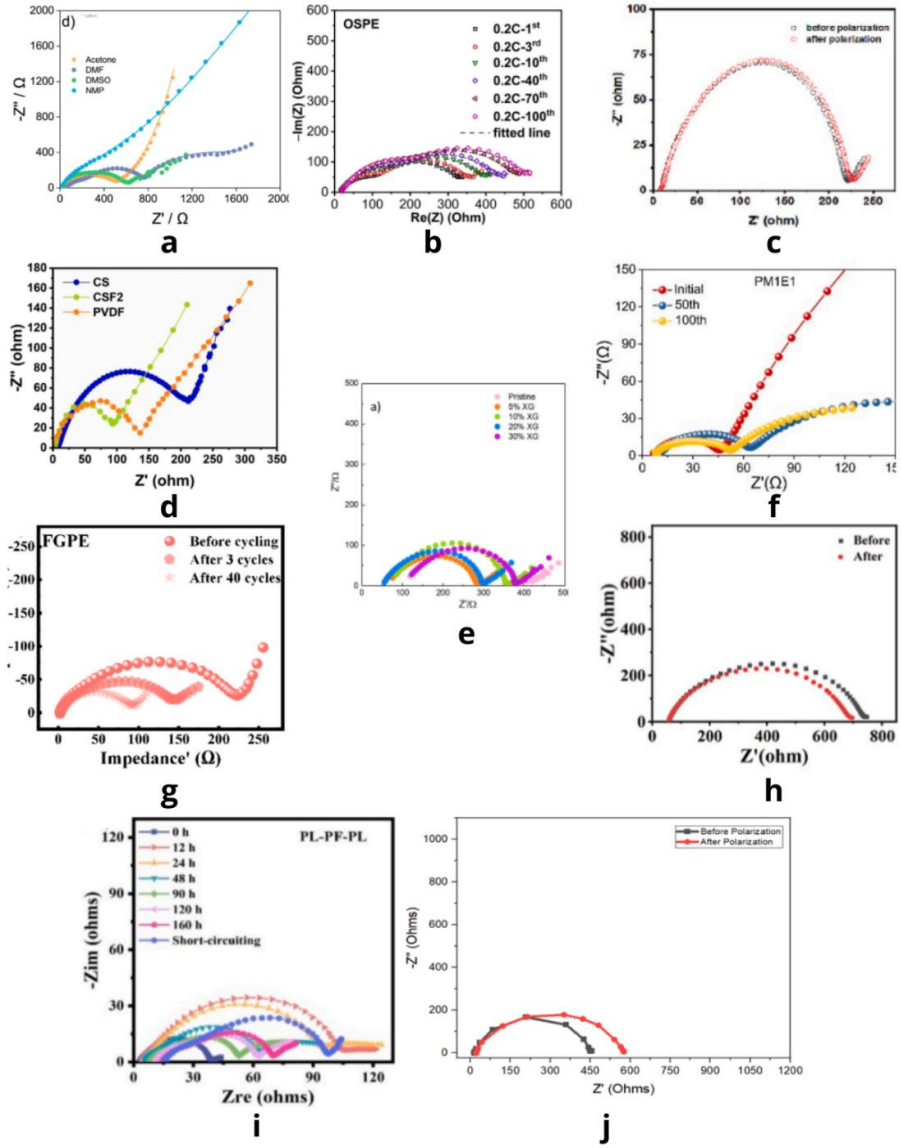

Figure 3. EIS results of [a] SPEs (Pinto et al., 2026), [b] semi-IPN PEO-based SPEs (Nguyen et al., 2025), [c] TPVFP (Hu et al., 2026), [d] CSF_2 (Muhainia et al., 2026), [e–f] Li||NCM811 (Chen et al., 2026), [g] FGPE (Ge et al., 2026), [h] LIPTAQ (Kong et al., 2026), [i] Li|PL-PF-PL|$LiFePO_4$ (Feng et al., 2026), and [j] GPE (Sabir et al., 2026).

Table 2. Relationship Between Polymer Utilization and Solution Resistance (Rs) and Charge Transfer Resistance (Rct) in Lithium Batteries

Material	Rct(Ω)	Rs(Ω)	Reference
solid polymer electrolytes (SPEs)	200 - 260	8 - 20	Pinto et al., 2026
PE/C/$Al(OH)_3$	-	-	Wan et al., 2026
poly (acrylic acid)-polyamide (PA) + (PES)	-	-	Wang et al., 2026
CS, PVDF, CSF2	-	-	Mahaninia et al., 2026
PEO/ LiTFSI (EO/Li 1:21)	-	-	Patriarchi et al., 2026
CoTP@CC–Li	10.75	-	Kim et al., 2026
LiNbO3 coated LiCoO2 + Li Polimer	-	-	Thompson et al., 2025
semi-IPN PEO-based SPEs	-	-	Nguyen et al., 2025
FGPE	97	-	Ge et al., 2026
Li||NCM811	44.2	-	Chen et al., 2026
Li|PL-PF-PL|LiFePO4	-	-	Feng et al., 2026
PDE-PF	-	-	Ren et al., 2026
GPE	-	-	Sabir et al., 2026
PVFP dan TPVFP	-	-	Hu et al., 2026
LiPTAQ	-	-	Kong et al., 2026

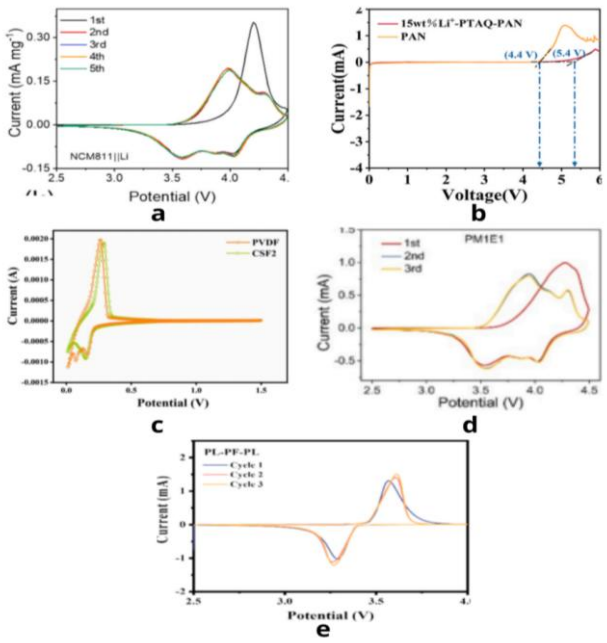

Figure 4. Cyclic voltammetry (CV) results of [a] PDE-PF (Ren et al., 2026), [b] LIPTAQ (Kong et al., 2026), [c] CSF_2 (Muhainia et al., 2026), [d] Li||NCM811 (Chen et al., 2026), and [e] Li|PL-PF-PL|$LiFePO_4$ (Feng et al., 2026).

3.1.5. Fabrication Methods

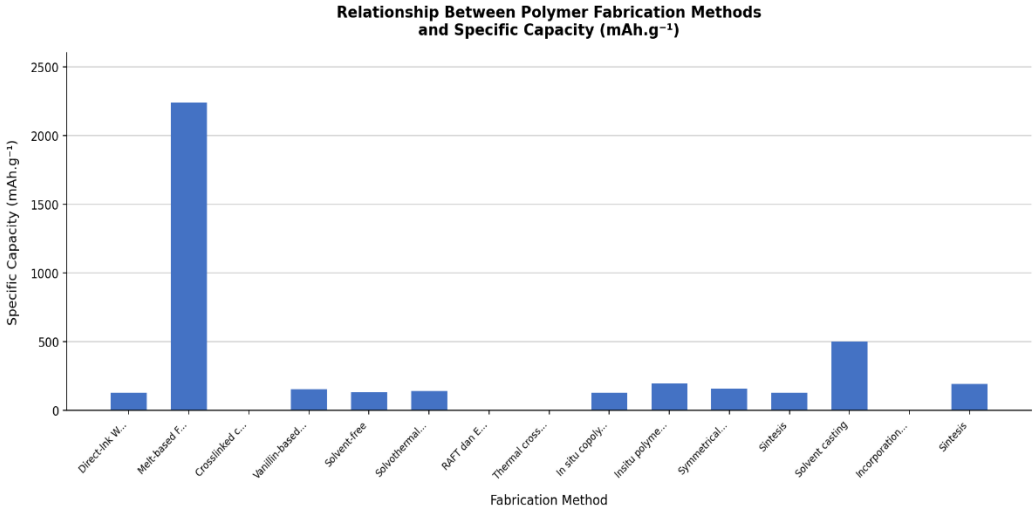

Graph 1. Relationship between polymer fabrication methods and specific capacity.

Based on Graph 1 and Table 3, the use of the melt-based fabrication method yields the highest specific capacity, reaching 2237 mAh g^{-1} for the PE/C/$Al(OH)_3$ material. Meanwhile, gel polymer electrolytes (GPEs) fabricated via the solvent casting method provide a specific capacity of 500 mAh g^{-1}, making it the second-highest value after the melt-based fabrication approach.

In addition, other methods such as direct ink writing, solvothermal synthesis, in situ copolymerization, in situ polymerization, symmetrical modification, and conventional synthesis yield specific capacities in the range of 130–190 mAh g^{-1}.

Although the literature indicates such variations in performance across fabrication methods, the choice of material also plays a critical role in determining the resulting specific capacity. This is supported by the findings presented in Figures 1, 2, 3, and 4, as well as Tables 1 and 2, which collectively confirm that polymer material utilization significantly influences crystallinity, crystallite size, surface area, morphology, solution resistance (Rs), charge-transfer resistance (Rct), and electrochemical performance.

Table 3. Relationship Between Polymer Fabrication Methods and Specific Capacity, Energy Density, and Power Density

Polymer Material	Method	Specific Capacity ($mAh.g^{-1}$)	Energy Density ($Wh\ kg^{-1}$)	Power Density (W/kg)	Reference
Solid Polymer Electrolytes (SPEs)	Direct-Ink Writing	128	-	-	Pinto et al., 2026
PE/C/$Al(OH)_3$	Melt-Based Fabrication	2237	-	-	Wan et al., 2026
Poly (Acrylic Acid)-Polyamide (PA)+(PES)	Crosslinked Cyclodextrin-Cellulose	-	-	-	Wang et al., 2026
CS, PVDF, CSF2	Vanillin-Based Cross-Linker (Vc)	40, 129, 154	-	-	Mahaninia et al., 2026
PEO/ LiTFSI (EO/Li 1:21)	Solvent-Free	130	-	-	Patriarchi et al., 2026
CoTP@CC–Li	Solvothermal Synthesis	142.0	-	-	Kim et al., 2026
LiNbO3 + LiCoO2 + Poly (ethylene glycol)	Raft Dan Enkapsulasi Polimerisasi	-	-	-	Thompson et al., 2025
Semi-IPN PEO-based SPEs	Thermal Cross-Linking	-	-	-	Nguyen et al., 2025
FGPE	In Situ Copolymerization	129	-	-	Ge et al., 2026
Li||NCM811	Insitu Polymerized	197.9	-	-	Chen et al., 2026
Li|PL-PF-PL|LiFePO4	Symmetrical Modification	133.98 - 155.96	-	-	Feng et al., 2026
PDE-PF	Sintesis	128.5	-	-	Ren et al., 2026
GPE	Solvent Casting	500	-	-	Sabir et al., 2026
PVFP dan TPVFP	Incorporation Fluoroether	-	-	-	Hu et al., 2026
LiPTAQ	Sintesis	190.9	-	-	Kong et al., 2026

3.2. Use of Polymers in Lithium Batteries

3.2.1. X-Ray Diffraction (XRD)

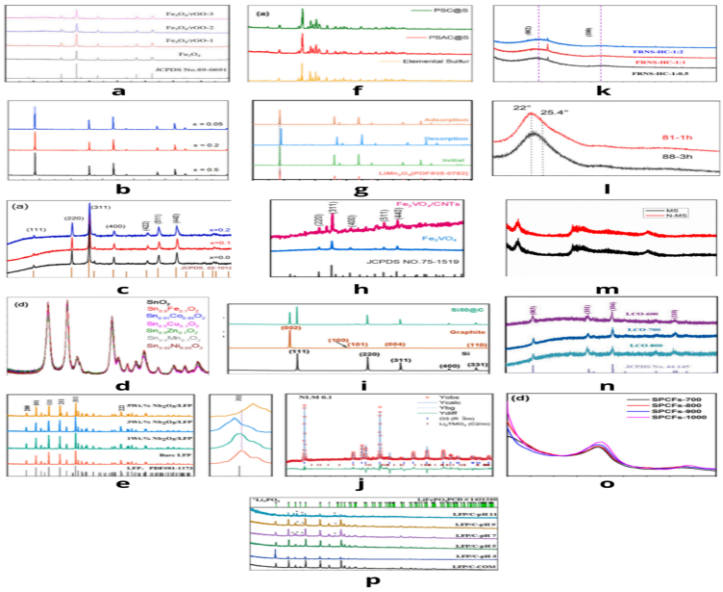

Figure 5. XRD results of [a] Fe_3O_4, Fe_3O_4/rGO (Han et al., 2026), [b] $Li_4-x/3Ti_5-2x/3Cr_xO_{12}$ (Nasara et al., 2026), [c] $Zn_1-xCo_xFe_2O_4$ (Hussain et al., 2026), [d] pristine and doped SnO_2 (Fe, Co, Cu, Zn, Mn, Ni) (Lübke et al., 2017), [e] Nb_2O_5/$LiFePO_4$ (Tang et al., 2026), [f] PSC@S (Almoguera et al., 2026), [g] $LiMn_2O_4$/C/PVDF (Chen et al., 2026), [h] Fe_2VO_4/CNTs (Meng et al., 2026), [i] Si_{50}@C (Pan et al., 2026), [j] $Na_{0.8}-xLi_xMn_{0.5}Fe_{0.3}Cu_{0.1}Ni_{0.1}O_2$ (Krishnan et al., 2026), [k] FRNS–HC–1 (Guo et al., 2024), [l] N-doped carbon/SiOC (Monje et al., 2021), [m] N-doped MoS_2 (Li et al., 2019), [n] LCO (Zeng et al., 2026), [o] SPCFs (Jin et al., 2022), and [p] synthesized LFP/C (Nekahi & Zaghib, 2020).

X-ray diffraction (XRD) data serve as an important parameter for validating the success of mixing approaches such as synthesis, doping, and composite formation. In addition, XRD analysis is essential for understanding crystallinity, crystal phases, purity, and crystallite size; therefore, it plays a crucial role in material characterization.

Based on the literature data compiled in Figure 5 (a–p), most samples exhibit sharp diffraction peaks, indicating a strong crystalline nature in lithium battery materials, both in electrodes and electrolytes. However, this is not universal, as Figures 5 (k–o) predominantly show amorphous structures. The formation of crystalline or amorphous phases is strongly influenced by the applied methods, such as synthesis, doping, and composite engineering. In addition, the elemental composition of the base material also plays a significant role.

These structural characteristics are closely related to electrochemical performance. Considering the ion transport processes during charge and discharge cycles, crystal structure becomes a key factor governing ion mobility and their interaction with the electrode materials.

3.2.2. Morphology

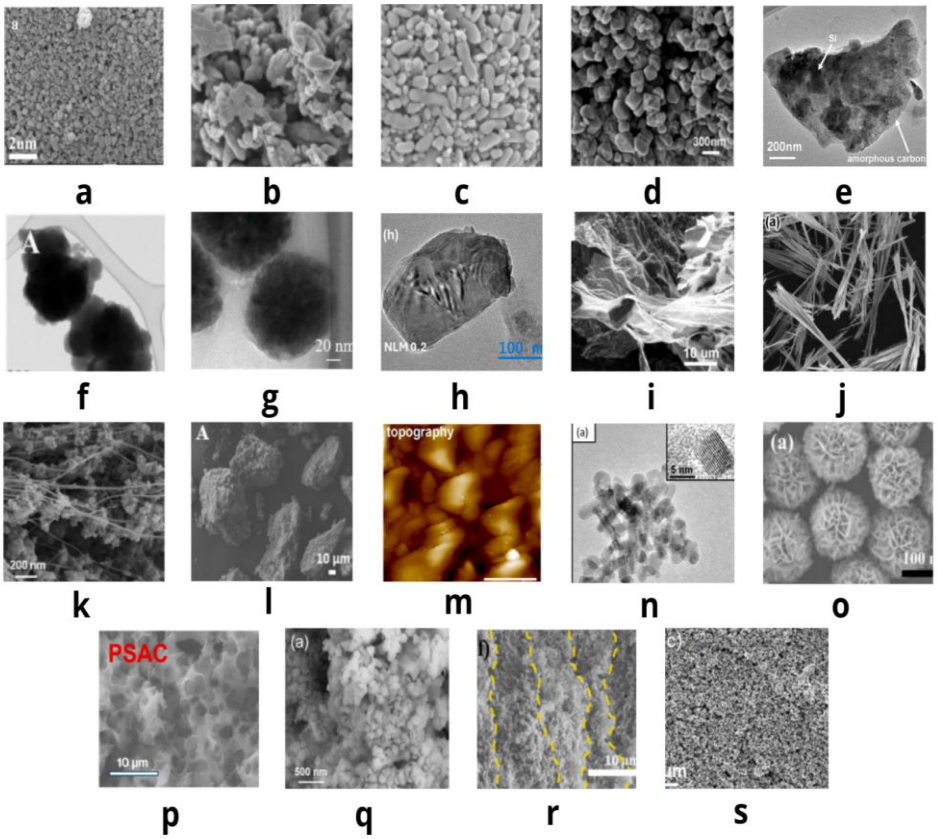

Figure 6. Morphological analysis based on SEM, EDX, and TEM data of [a] Nb_2O_5/$LiFePO_4$ (Tang et al., 2026), [b–c] LFP/C synthesized via pH variation and hydrothermal synthesis (Nekahi & Zaghib, 2026), [d] $LiMn_2O_4$/C/PVDF (Chen et al., 2026), [e] Si_{50}@C (Pan et al., 2026), [f] N-doped carbon/SiOC (Monje et al., 2021), [g] Fe_3O_4, Fe_3O_4/rGO (Han et al., 2026), [h] $Na_{0.8}-xLi_xMn_{0.5}Fe_{0.3}Cu_{0.1}Ni_{0.1}O_2$ (Krishnan et al., 2026), [i] FRNS–HC–1 (Guo et al., 2024), [j] SPCFs (Jin et al., 2022), [k] Fe_2VO_4/CNTs (Meng et al., 2026), [l] N-doped carbon/SiOC (Monje et al., 2021), [m] $Li_4-x/3Ti_5-2x/3Cr_xO_{12}$ (Nasara et al., 2026), [n] pristine and doped SnO_2 (Fe, Co, Cu, Zn, Mn, Ni) (Lübke et al., 2017), [o] N-doped MoS_2 (Li et al., 2019), [p] PSC@S (Almoguera et al., 2026), [q] $Zn_1-xCo_xFe_2O_4$ (Hussain et al., 2026), [r] CMC-CS/LFP (Shen et al., 2026), and [s] $LiFePO_4$@LCO (Zeng et al., 2026).

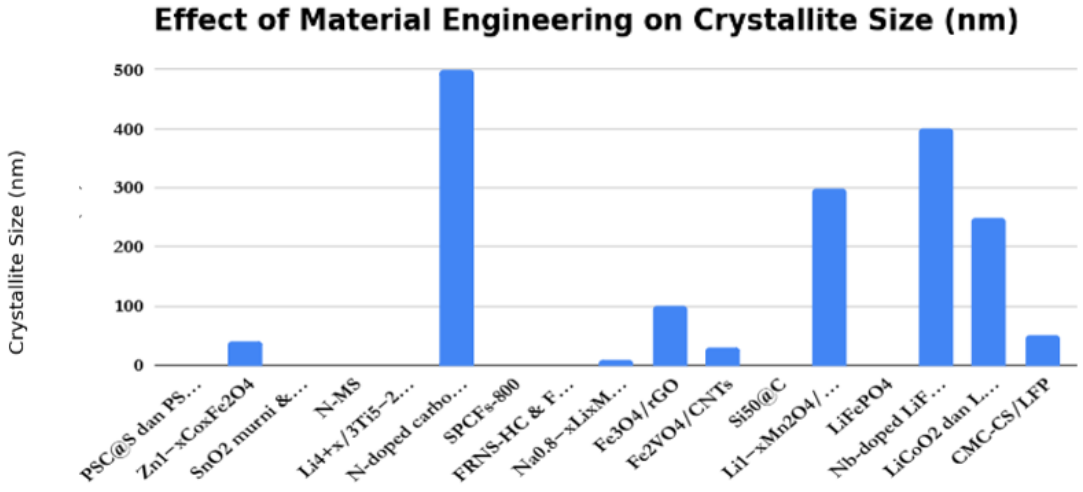

(a)

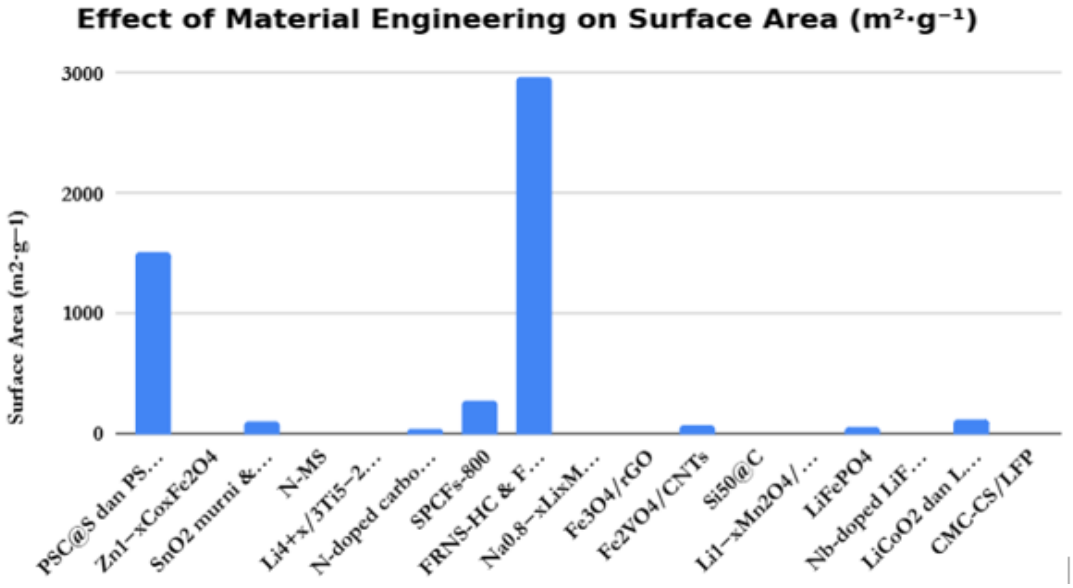

(b)

Graph 2. Relationship Between the Use of Non-Polymer Materials and [a] Crystallite Size, [b] Surface Area

Table 4. Relationship Between Non-Polymer Materials and Crystallinity and Surface Area Results

Material	Crystallite Size (nm)	Surface Area ($m^2\ g^{-1}$)	Reference
PSC@S dan PSAC@S	-	394 - 1518	Almoguera et al., 2026
$Zn_{1-x}Co_xFe_2O_4$ ($0 \le x \le 0.2$)	40.83 - 38.53	-	Hussain et al., 2026
SnO2 Doping (Fe, Co, Cu, Zn, Mn, Ni)	6.8	95 - 102	Lübke et al., 2017
N-MS	-	-	Li et al., 2019
$Li_{4+x}/_3Ti_{5-2x}/_3Cr_xO_{12}$, x = 0.5	-	-	Nasara et al., 2026
N-doped carbon/SiOC	500	33 - <5	Monje et al., 2021

Material	Crystallite Size (nm)	Surface Area ($m^2 g^{-1}$)	Reference
SPCFs-800	-	281 - 244	Jin et al., 2022
FRNS-HC- 1:2 dan FRNS-AC-1:2	-	2602.630 - 2961.260	Guo et al., 2024
$Na_{0.8}Li_{0.1}Mn_{0.4}Fe_{0.3}Cu_{0.1}Ni_{0.1}O_2$	9 nm	-	Krishnan et al., 2026
Fe3O4/rGO	9.7, 9.2, 8.7	-	Han et al., 2026
Fe2VO4/CNTs	10 - 30	69.12	Meng et al., 2026
Si50@C	-	-	Pan et al., 2026
Li1-xMn2O4/C/PVDF	300	-	Chen et al., 2026
$LiFePO_4$	-	12.6 - 52.1	Nekahi & Zaghib 2026
Nb-doped $LiFePO_4$/C	200 - 400	-	Tang et al., 2026
LiCoO2 dan LCO	250	56.6 - 110.72	Zeng et al., 2026
CMC-CS/LFP	50	-	Shen et al., 2026

The use of instrumentation such as SEM, TEM, and FESEM plays an important role in understanding the effects of synthesis, doping, and composite formation on the resulting morphology, including dimensions, porosity, and particle phase distribution. In Figures 6(a), (c), and (d), the materials predominantly exhibit small granular spherical structures, with some particles appearing elongated, compact, and polycrystalline. In contrast, Figures 6(p), (q), and (r) show network-like structures resembling cotton-like morphologies.

Figure 6(o) displays microspherical structures with flower-like morphology, while Figures 6(j) and (k) show wire- or needle-like structures that are interconnected and cross-linked. Figure 6(p) exhibits a well-ordered macroporous structure (PSAC). When grouped based on mixing methods, Figures 6(a), (h), (i), (j), (l), (m), (n), (o), and (q) correspond to morphologies obtained via doping processes, where the resulting structures vary widely, including granular particles, fibrous networks, flower-like fibers, solid rock-like formations, and sponge-like aggregates.

Meanwhile, Figures 6(b), (c), (d), (e), (f), (g), (k), (p), (r), and (s) represent morphologies derived from composite-based approaches, which include both granular and sponge-like structures. Figures 6(b) and (c) are specifically associated with synthesis-derived morphologies characterized by granular particles. In particular, Figure 6(m) represents surface topography analysis obtained using Atomic Force Microscopy (AFM), which reveals nanoscale surface roughness.

The morphological structures shown in Figures 6(a), (h), (i), (j), (l), (m), (n), (o), and (q) are predominantly crystalline in nature, as also supported by the XRD results in Figure 5(b), (c), (d), (e), (j), (k), (l), and (o). A similar trend is observed for composite-based materials. The synergy between porous structures (facilitating ion transport) and carbon or nanowire networks (facilitating electron transport) is a key factor in enhancing reversible capacity and cycling stability in lithium battery systems reported in this review.

3.2.3. Electrochemical Impedance Spectroscopy (EIS)

Electrochemical Impedance Spectroscopy (EIS) is a key technique for understanding charge transport kinetics. In general, EIS spectra consist of a semicircular region (high-to-mid frequency range) and an inclined line (low-frequency region). The ohmic resistance (Rs) is indicated by the intercept of the curve with the real axis (Z′) at the highest frequency.

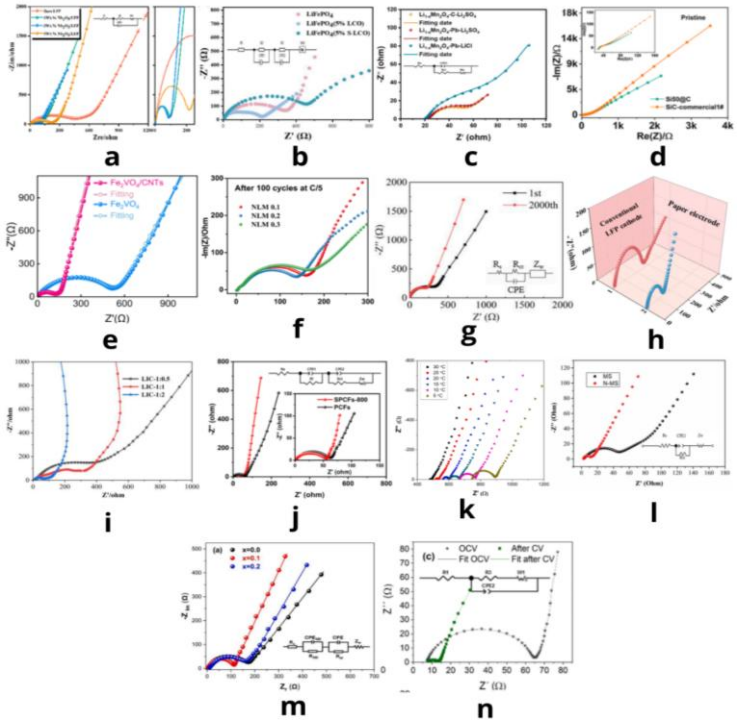

Figure 7. EIS resistance and capacity plots of [a] Nb_2O_5/$LiFePO_4$ (Tang et al., 2026), [b] $LiFePO_4$@LCO (Zeng et al., 2026), [c] $LiMn_2O_4$/C/PVDF (Chen et al., 2026), [d] Si_{50}@C (Pan et al., 2026), [e] Fe_2VO_4/CNTs (Meng et al., 2026), [f] $Na_{0.8}$−x$Li_x$$Mn_{0.5}$$Fe_{0.3}$$Cu_{0.1}$$Ni_{0.1}O_2$ (Krishnan et al., 2026), [g] Fe_3O_4, Fe_3O_4/rGO (Han et al., 2026), [h] CMC-CS/LFP (Shen et al., 2026), [i] FRNS–HC–1 (Guo et al., 2024), [j] SPCFs (Jin et al., 2022), [k] Li_4−x/3Ti_5−2x/3Cr_xO_{12} (Nasara et al., 2026), [l] N-doped MoS_2 (Li et al., 2019), [m] Zn_1−x$Co_xFe_2O_4$ (Hussain et al., 2026), and [n] PSC@S (Almoguera et al., 2026).

Table 5. Effect of Non-Polymer Materials on Solution Resistance (Rs) and Charge Transfer Resistance (Rct) in Lithium Batteries

Material	Rct(Ω)	Rs(Ω)	Referensi
PSC@S dan PSAC@S	-	-	Almoguera et al., 2026
$Zn_{1-x}Co_xFe_2O_4$ ($0 \le x \le 0.2$)	-	-	Hussain et al., 2026
SnO2 murni dan Doping (Fe, Co, Cu, Zn, Mn, Ni)	-	-	Lübke et al., 2017
N-MS	50.68	6.85	Li et al., 2019
$Li_{4+x}/_3Ti_{5-2x}/_3Cr_xO_{12}$, x = 0.5	5.52	-	Nasara et al., 2026
N-doped carbon/SiOC	-	-	Monje et al., 2021
SPCFs-800	-	49.9	Jin et al., 2022
FRNS-HC- 1:2 dan FRNS-AC-1:2	-	-	Guo et al., 2024
$Na_{0.8}Li_{0.1}Mn_{0.5}Fe_{0.3}Cu_{0.1}Ni_{0.1}O2$	-	-	Krishnan et al., 2026
Fe3O4/rGO	186	2.3	Han et al., 2026
Fe2VO4/CNTs	-	-	Meng et al., 2026
Si50@C	-	-	Pan et al., 2026
Li1-xMn2O4/C/PVDF	-	-	Chen et al., 2026
$LiFePO_4$	-	-	Nekahi & Zaghib 2026
Nb-doped $LiFePO_4$/C	2.24	86.18	Tang et al., 2026
LiCoO2 dan LCO	-	-	Zeng et al., 2026
CMC-CS/LFP	138	-	Shen et al., 2026

The EIS results in Figure 7(l) show a significant shift in the Rs values with variations in temperature, where lower temperatures lead to an increase in electrolyte resistance. Charge transfer resistance (Rct), represented by the diameter of the semicircle in the Nyquist plot, reflects the resistance encountered by electrons crossing the electrode–electrolyte interface.

In Figures 7(e) and 7(f), the addition of CNTs or modifications in NLM significantly reduces the semicircle diameter compared to the pristine materials. This indicates improved electrical conductivity and faster redox kinetics. Nearly all panels in Figure 7(a), (b), (c), (g), (j), (l), and (m) include an equivalent electrical circuit (EEC) inset used for fitting the experimental impedance data.

3.2.4. Cyclic Voltammetry (CV)

Cyclic Voltammetry (CV) characterization is widely used to analyze redox reactions, electrochemical reversibility, and charge-transfer kinetics in energy storage systems. Based on the current–potential profiles in Figure 8(a–n), several observations can be made. Most materials exhibit well-defined anodic (oxidation) and cathodic (reduction) peaks, indicating the presence of Faradaic reactions.

In Figures 8(a), (f), and (l), sharp peaks are observed in the first cycle, which subsequently shift or decrease in intensity in later cycles, indicating lithiation and delithiation processes. Structural stability during cycling can be evaluated through the overlap of CV curves across different cycles.

Figures 8(a) and 8(f) show nearly overlapping CV curves between the second and third cycles, indicating excellent electrochemical reversibility and strong structural stability during lithium-ion intercalation and deintercalation processes.

Furthermore, Figure 8(i) demonstrates that doping SnO_2 with various transition metals (Fe, Co, Cu, Zn, Mn, Ni) alters the area under the CV curve, which is directly correlated with the resulting charge storage capacity.

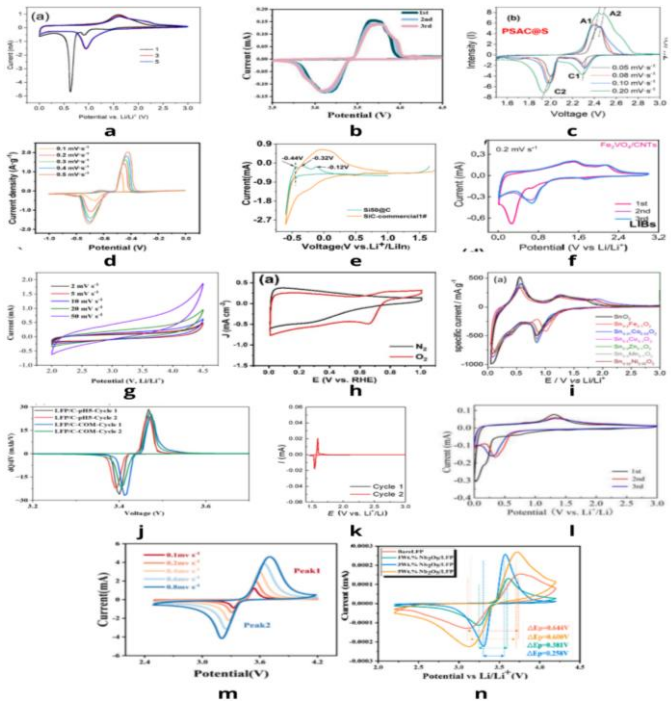

Figure 8. Redox reaction kinetics, reaction mechanism, and potential window from CV data of [a] $Zn_1-xCo_xFe_2O_4$ (Hussain et al., 2026), [b] $LiFePO_4$@LCO (Zeng et al., 2026), [c] PSC@S (Almoguera et al., 2026), [d] $LiMn_2O_4$/C/PVDF (Chen et al., 2026), [e] Si_{50}@C (Pan et al., 2026), [f] Fe_2VO_4/CNTs (Meng et al., 2026), [g] FRNS–HC–1 (Guo et al., 2024), [h] SPCFs (Jin et al., 2022), [i] Fe_3O_4, Fe_3O_4/rGO (Han et al., 2026), [j] synthesized LFP/C (Nekahi & Zaghib, 2020), [k] $Li_4-x/3Ti_5-2x/3Cr_xO_{12}$ (Nasara et al., 2026), [l] pristine and doped SnO_2 (Fe, Co, Cu, Zn, Mn, Ni) (Lübke et al., 2017), [m] CMC-CS/LFP (Shen et al., 2026), and [n] Nb_2O_5/$LiFePO_4$ (Tang et al., 2026).

The effect of scan rate variation from low to high, as shown in Figures 8(c), 8(d), 8(g), and 8(m), provides insight into ion-transport kinetics. Peak shifting behavior is observed, where increasing scan rates cause the anodic peaks to shift toward more positive potentials, while cathodic peaks shift toward more negative potentials. This behavior indicates increased polarization at higher scan rates.

In addition, pseudocapacitive contributions are evident. As shown in Figure 8(g), the CV curves largely maintain their shape even at a high scan rate of 50 mV s^{-1}, indicating significant surface-controlled charge storage (pseudocapacitance). This behavior enables excellent high-rate performance due to rapid and reversible charge storage mechanisms.

3.2.5. Methods

Table 4 and Graph 4 confirm the effectiveness of various methods such as composite engineering, doping, and synthesis. For non-polymer materials, the highest specific capacity is achieved through composite-based approaches, highlighting their effectiveness in improving energy-storage performance.

However, Graph 4 also indicates that relatively high specific capacities are more frequently observed in doping-based approaches compared with composite-based methods. It is important to emphasize that, based on this literature review, the performance outcomes of composites and doping strategies are not universally conclusive.

In other words, when the same material system is modified using different methods, doping does not necessarily outperform composites in terms of specific capacity, and vice versa. Therefore, the superiority of a given method is highly dependent on material composition, synthesis conditions, and system-specific interactions rather than the method itself alone.

4. Conclusion

In this study, a comparison has been conducted between the use of polymers and mixed/non-polymer materials (synthesis, doping, and composite systems) in lithium battery applications. From the characterization results, X-ray diffraction (XRD) indicates that polymeric materials tend to form amorphous structures. In particular, LIPTAQ, PVFP, and TPVFP are polymer materials that exhibit crystalline characteristics. In contrast, non-polymer materials or element-based systems prepared through mixing methods (synthesis, doping, and composites) generally show predominantly crystalline XRD patterns, as evidenced by sharp diffraction peaks rather than amorphous features, as observed in materials such as FRNS–HC–1, N-doped carbon/SiOC, N-doped MoS_2, LCO, and SPCFs.

On the other hand, morphological characterization using SEM, TEM, and EDX reveals similarities between polymer and non-polymer systems. Both systems exhibit comparable morphological features, including small granular structures, fibrous networks, flower-like aggregates, large granules, rock-like particles, sponge-like porous structures, dense porous frameworks, and other similar morphologies. This confirms that morphological characteristics are not exclusively dependent on whether the material is polymeric or non-polymeric.

Electrochemical results further indicate that polymer-based materials achieve the highest specific capacity, reaching up to 2237 mAh g^{-1}, followed by 500 mAh g^{-1}, and then a range of 190–130 mAh g^{-1}. In comparison, non-polymer materials do not exhibit the highest specific capacity values. However, their average performance remains relatively high, ranging from 125 to 1000 mAh g^{-1}. This suggests that non-polymer materials are, on average, more effective in providing stable and substantial improvements in lithium battery performance.

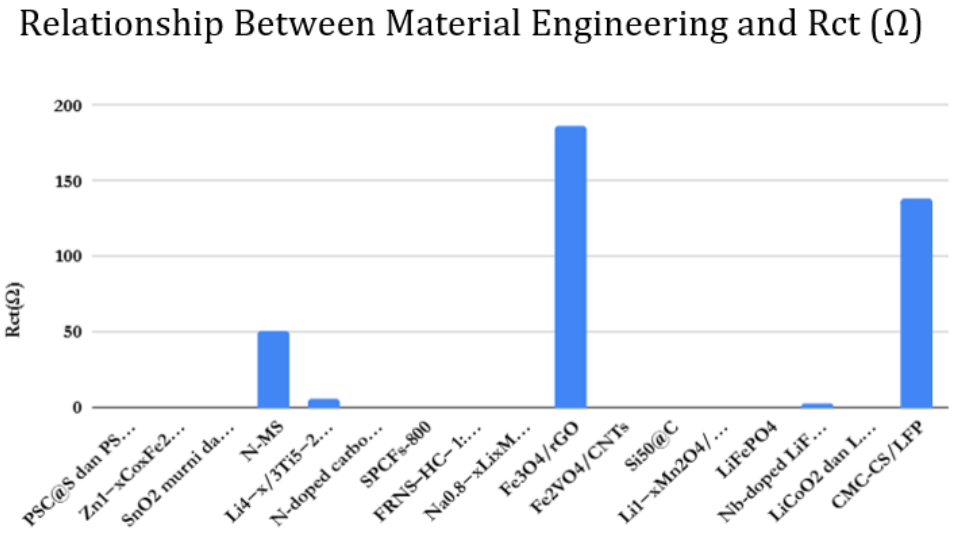

(a)

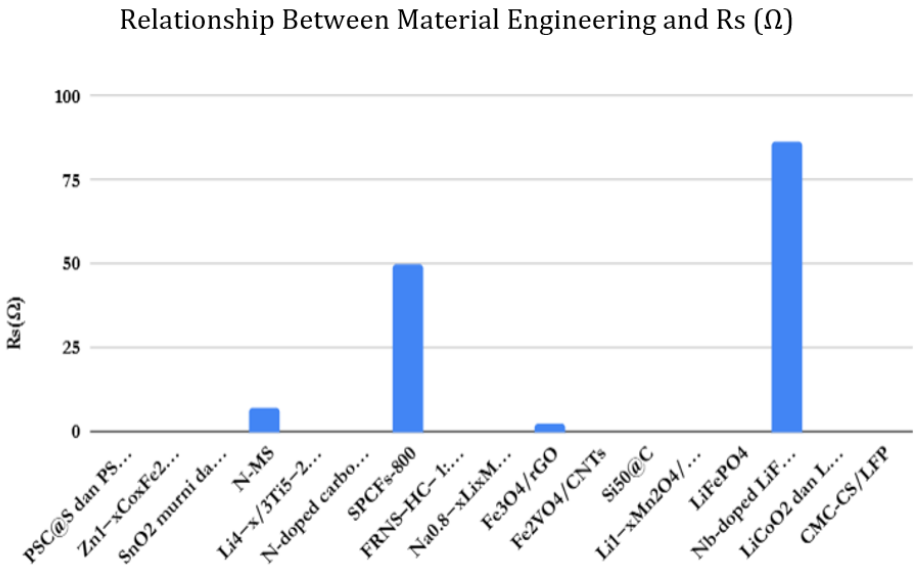

(b)

Figure 3. Relationship between the use of non-polymer materials and solution resistance (Rs) and charge transfer resistance (Rct) in lithium batteries.

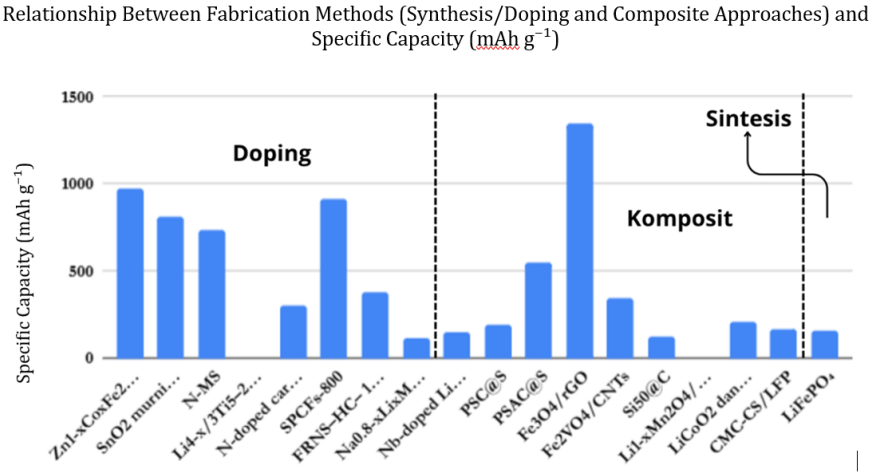

Figure 4. Relationship between synthesis, doping, and composite methods and specific capacity.

Table 5. Relationship Between Synthesis, Doping, and Composite Methods and Specific Capacity, Power Density, and Energy Density

Material	Method	Specific Capacity (mAh g^{-1})	Energy Density (Wh kg^{-1})	Power Density (W kg^{-1})	Reference
PSC@S dan PSAC@S	Synthesis- Composite	190 - 550	-	-	Almoguera et al., 2026
$Zn_{1-x}Co_xFe_2O_4$ ($0 \leq x \leq 0.2$)	Doping	970.1	-	-	Hussain et al., 2026
Pristine SnO_2 and Doping (Fe, Co, Cu, Zn, Mn, Ni)	Synthesis- Composite	812 - 953	-	-	Lübke et al., 2017
N-MS	Doping	738	-	-	Li et al., 2019
$Li_{4+x}/_3Ti_{5-2x}/_3Cr_xO_{12}$, x = 0.5	Doping	-	-	-	Nasara et al., 2026
N-doped carbon/SiOC	Doping	300	-	-	Monje et al., 2021
SPCFs-800	Doping	910	-	-	Jin et al., 2022
FRNS-HC- 1:2 dan FRNS-AC-1:2	Doping	374.2	147.67	-	Guo et al., 2024
$Na_{0.8}Li_{0.1}Mn_{0.5}Fe_{0.3}Cu_{0.1}Ni_{0.1}O_2$	Doping	115.3	-	-	Krishnan et al., 2026
Fe3O4/rGO	Composite	1349	-	-	Han et al., 2026
Fe2VO4/CNTs	Composite	348.4	-	-	Meng et al., 2026
Si50@C	Composite	125	-	-	Pan et al., 2026
Li1-xMn2O4/C/PVDF	Composite	-	-	-	Chen et al., 2026
$LiFePO_4$	Synthesis (Hidrotermal)	155	123	-	Nekahi & Zaghib 2026
Nb-doped $LiFePO_4$/C	Doping	145.1	-	-	Tang et al., 2026
LiCoO2 dan LCO	Composite	206	578 - 290	-	Zeng et al., 2026
CMC-CS/LFP	Composite	165	-	-	Shen et al., 2026

References

Awan, H. T. A., Abdah, M. a. a. M., Mehar, M., Walvekar, R., Chaudhary, V., Khalid, M., & Khosla, A. (2024). MXene-polymer hybrid composites for advanced energy storage: Insights into supercapacitors and batteries. Journal of Energy Storage, 95, 112449. https://doi.org/10.1016/j.est.2024.112449

Cardoso-Almoguera, A., Tesio, A. Y., Amaro-Gahete, J., Gómez-Cámer, J. L., Benítez, A., & Caballero, A. (2026). Hierarchical microporous nitrogen self-doped carbon derived from biomass as a multifunctional material for beyond lithium-ion batteries. Materials Today Chemistry, 53, 103518. https://doi.org/10.1016/j.mtchem.2026.103518

Chen, J., Gao, J., Zhang, R., Wang, Z., Ren, Q., Gao, F., Zhang, Z., Du, X., & Hao, X. (2026). Construction of Li1-xMn2O4-Pb composite electrode ESIX system for efficient lithium recovery from high-sodium sulfate-type lithium-precipitation mother liquor. Journal of Environmental Chemical Engineering, 14(3), 122690. https://doi.org/10.1016/j.jece.2026.122690

Chen, P., Zhang, H., Dong, S., Zhang, S., & Zhao, D. (2026). Non-flammable gel polymer electrolytes with stable dual-interface compatibility for safe and high-voltage lithium metal batteries. Journal of Colloid and Interface Science, 718, 140480. https://doi.org/10.1016/j.jcis.2026.140480

Chi, F., Shen, J., Liu, S., Pan, H., Quan, H., & Zhu, S. (2025). Fluorination of PEO-based polymer electrolytes and their application in solid-state lithium batteries. Advanced Nanocomposites, 3, 34–51. https://doi.org/10.1016/j.adna.2025.12.003

Cui, J., Shi, H., Song, X., Wang, X., Han, Y., & Liu, J. (2026). Molecular engineering of D-A type conjugated polymers consisting of thiophene and anthrarufin moieties for efficient electrochromism and energy storage. Polymer, 353, 129933. https://doi.org/10.1016/j.polymer.2026.129933

De Marco, A., Deville, Q., & Arbizzani, C. (2026). From synthesis to characterization: Advancing disordered rocksalts for cobalt-free lithium-ion batteries. Journal of Power Sources, 679, 240210. https://doi.org/10.1016/j.jpowsour.2026.240210

Feng, Y., Deng, L., Zhang, Z., Li, J., Lu, F., Chen, R., Yang, R., Xie, G., Ke, X., & Xiao, R. (2026). A novel sandwich-structure polymer gel electrolyte with high ionic conductivity and safety for lithium metal batteries. Journal of Energy Storage, 167, 122551. https://doi.org/10.1016/j.est.2026.122551

Ge, N., Gao, W., Cui, H., & Song, Y. (2026). Simultaneously boosting cycle life and safety of lithium metal batteries through synergistic interphase engineering with gel polymer and fluoroethylene carbonate. Journal of Power Sources, 678, 240048. https://doi.org/10.1016/j.jpowsour.2026.240048

Ge, N., Gao, W., Cui, H., & Song, Y. (2026b). Simultaneously boosting cycle life and safety of lithium metal batteries through synergistic interphase engineering with gel polymer and fluoroethylene carbonate. Journal of Power Sources, 678, 240048. https://doi.org/10.1016/j.jpowsour.2026.240048

Gong, Y., Liu, T., Yang, K., Zhong, M., Luo, K., Chen, Y., Lu, J., Lei, W., Liu, D., Guo, C., & Ma, A. (2026). Novel quasi-solid batteries with In-Situ originated from gel polymer electrolyte. Chemical Engineering Science, 332, 124057. https://doi.org/10.1016/j.ces.2026.124057

Guo, X., Qiao, Y., Yi, Z., Pedersen, C. M., Wang, Y., Tian, X., & Han, P. (2023). Furfural residues derived nitrogen-sulfur co-doped sheet-like carbon: An excellent electrode for dual carbon lithium-ion capacitors. Green Energy & Environment, 9(9), 1427–1439. https://doi.org/10.1016/j.gee.2023.05.007

Han, X., Wang, Z., He, Y., Zhang, R., Ruan, P., Zhang, L., Zhang, T., An, C., & Deng, Q. (2026). Superparamagnetic Fe3O4/rGO composite as high-rate and high-safety electrode for lithium-ion battery. Materials Chemistry and Physics, 359, 132547. https://doi.org/10.1016/j.matchemphys.2026.132547

Hong, S., Lee, Y., Kim, H., Go, M. C., Kim, U., Sun, Y., & Kim, D. (2025). Redefining polymer binders: enabling ion transport and interfacial stability in sulfide-based all-solid-state lithium batteries. Energy Storage Materials, 83, 104756. https://doi.org/10.1016/j.ensm.2025.104756

Hong, S., Lee, Y., Kim, H., Go, M. C., Kim, U., Sun, Y., & Kim, D. (2025b). Redefining polymer binders: enabling ion transport and interfacial stability in sulfide-based all-solid-state lithium batteries. Energy Storage Materials, 83, 104756. https://doi.org/10.1016/j.ensm.2025.104756

Hu, L., Xiong, Q., Kang, C., Li, Y., Shi, Y., & Jiang, Y. (2026). Tailoring polymer phase regulation and solvation structure engineering enables stable lithium metal solid-state batteries. Chemical Engineering Journal, 536, 175962. https://doi.org/10.1016/j.cej.2026.175962

Hu, Y., Yu, Z., Tang, M., Li, H., Zhang, Q., Feng, Y., Wang, Y., Ye, M., & Liu, Q. (2026). Polymer electrolyte-mediated interfacial chemistry for high-performance lithium-ion batteries. Energy Storage Materials, 84, 104866. https://doi.org/10.1016/j.ensm.2025.104866

Hussain, M., Hussain, A., Hussain, A., Shah, W. A., Wang, S., Abbas, S. M., Son, Y., & Khan, M. T. (2026). Superior anode performance in lithium-ion batteries with optimized cobalt-doped zinc ferrite. Electrochemistry Communications, 188, 108170. https://doi.org/10.1016/j.elecom.2026.108170

Jin, P., Li, L., Gu, X., Hu, Y., Zhang, X., Lin, X., Ma, X., & He, X. (2022). S-doped porous carbon fibers with superior electrode behaviors in lithium ion batteries and fuel cells. Materials Reports Energy, 2(4), 100160. https://doi.org/10.1016/j.matre.2022.100160

Kim, J. S., Kim, Y., Baek, S. H., Jeon, Y., Kim, S., Kim, W. I., Kim, D. W., Lee, H., Huang, S., Kim, H. C., Lee, J., Lee, Y. M., Yamada, A., Park, J., & Park, H. S. (2025). Two-dimensional polymeric metal phthalocyanines with anion fluxing and Li-ion-conducting properties for lithium metal full batteries. eScience, 6(2), 100480. https://doi.org/10.1016/j.esci.2025.100480

Kong, Y., Tian, H., Che, Y., Pan, Z., Cai, Y., Yao, X., & Su, Z. (2026). Ordered lithium-ion channel in carbonyl-rich conjugated microporous polymer composite solid electrolytes for stable lithium batteries. Materials Today Chemistry, 53, 103452. https://doi.org/10.1016/j.mtchem.2026.103452

Krishnan, A., Joshi, A., Leifer, N., Mukherjee, A., Chakrabarty, S., & Noked, M. (2026). Structural and interfacial stabilization of sodium-deficient O3-type layered oxide cathodes via optimized lithium doping. Energy Storage Materials, 88, 105118. https://doi.org/10.1016/j.ensm.2026.105118

Lan, T., Feng, Y., He, M., Xu, W., Yin, Y., Li, Y., Li, F., Xiang, W., Long, J., & Hu, A. (2026). Precision functional group engineering in solid-state polymer electrolytes for lithium-metal batteries. Energy Storage Materials, 88, 105153. https://doi.org/10.1016/j.ensm.2026.105153

Li, S., Qu, D., Wang, P., Wang, Y., & Xie, F. (2019). N-doped MOS2 Nano-Flowers as High-Performance anode electrode for excellent lithium storage. International Journal of Electrochemical Science, 14(8), 7507–7515. https://doi.org/10.20964/2019.08.35

Li, X., Zhao, Z., Yuan, S., Cheng, J., Hou, W., Hou, L., Liu, F., & Yuan, C. (2026). Emerging of dual-atom electrocatalysts advancing lithium-sulfur batteries: recent advances, challenges and perspectives. Energy Storage Materials, 86, 104965. https://doi.org/10.1016/j.ensm.2026.104965

Liang, J., Wu, Y., Wang, S., & He, Z. (2026). Highly conductive polymer electrolytes for solid-state lithium batteries: From mechanisms to applications. Sustainable Energy Technologies and Assessments, 86, 104840. https://doi.org/10.1016/j.seta.2026.104840

Liu, J., Deng, B., Liu, M., Zhang, Y., Yang, Z., Huang, T., & Liu, H. (2026). Zwitterionic polyurethane-based solid polymer electrolytes for high-performance solid-state Lithium metal batteries. Chemical Engineering Journal, 537, 176580. https://doi.org/10.1016/j.cej.2026.176580

Lübke, M., Ning, D., Armer, C. F., Howard, D., Brett, D. J., Liu, Z., & Darr, J. A. (2017). Evaluating the potential benefits of metal ion doping in SNO 2 negative electrodes for lithium ion batteries. Electrochimica Acta, 242, 400–407. https://doi.org/10.1016/j.electacta.2017.05.029

Luo, Y., Zhang, C., Liao, Y., Ding, Z., Li, D., Zhu, L., Luo, H., Liu, B., Guo, J., Peng, X., Song, S., Xiang, Y., & Xie, D. (2026). In-situ radical polymerization for solid polymer electrolytes in lithium-ion batteries: a comprehensive review. Chemical Engineering Journal, 537, 176332. https://doi.org/10.1016/j.cej.2026.176332

Mahaninia, M. H., Rathi, K., Yan, N., Sain, M., & Van Der Kuur, C. (2025). Self-healable chitosan-based polymer binder for anode in lithium-ion batteries. Chemical Engineering Journal, 528, 172151. https://doi.org/10.1016/j.cej.2025.172151

Meng, L., Hao, Z., Cui, Y., An, L., Zhang, Y., Wu, Q., Cui, S., Peng, J., & Chen, H. (2026). High-performance electrodes for lithium-ion and sodium-ion batteries: Preparation and electrochemical properties of Fe2VO4/carbon nanotube composites. Journal of Alloys and Compounds, 1065, 188058. https://doi.org/10.1016/j.jallcom.2026.188058

Mohammadipour, E., & Gharahcheshmeh, M. H. (2025). Corrosion and protection in lithium-ion and sodium-ion batteries: Principles and applications of graphene and conducting polymers as anticorrosion coatings. Next Research., 2(4), 100789. https://doi.org/10.1016/j.nexres.2025.100789

Monje, I. E., Sanchez-Ramirez, N., Santagneli, S. H., Camargo, P. H., Bélanger, D., Schougaard, S. B., & Torresi, R. M. (2021). In situ-formed nitrogen-doped carbon/silicon-based materials as negative electrodes for lithium-ion batteries. Journal of Electroanalytical Chemistry, 901, 115732. https://doi.org/10.1016/j.jelechem.2021.115732

Nasara, R. N., Lin, C., Govindarajan, K., Sosa, R. B., Pelegov, D., Hsu, W., Tsai, P., Takeshi, A., & Lin, S. (2025). Nanoclustering in Doped-Lithium Titanate and its Effects on Interfacial Electrochemical Kinetics. Applied Surface Science Advances, 34, 100991. https://doi.org/10.1016/j.apsadv.2026.100991

Nekahi, A., & Zaghib, K. (2025). Toward zero-waste and low-emissions in $LiFePO_4$ synthesis for sustainable lithium-ion batteries. Energy Storage Materials, 84, 104759. https://doi.org/10.1016/j.ensm.2025.104759

Nguyen, T. M., Biressaw, G. M., Kim, D. Y., Kim, D. W., Jo, H. W., Suk, J., & Kang, Y. (2025). Improved stability of solid polymer electrolyte using an additive for a 4 V lithium-ion battery operated at room temperature. Journal of Energy Storage, 126, 117098. https://doi.org/10.1016/j.est.2025.11709

Pan, Z., Liu, X., Liang, J., Ma, W., Liu, Z., Liang, Y., Zhu, S., Zhao, Y., & Gao, Z. (2026). High-performance silicon-carbon composite anode materials for all-solid-state lithium-ion batteries: adaptation to dry electrode process. Journal of Power Sources, 678, 240049. https://doi.org/10.1016/j.jpowsour.2026.240049

Pandit, B., Varez, A., & Huang, C. (2026). Polymer electrodes in solid-state metal-ion batteries: An in-depth review on recent advances, challenges, and future prospects. eScience Energy, 2(1), 100033. https://doi.org/10.1016/j.esen.2026.100033

Pandit, B., Varez, A., & Huang, C. (2026b). Polymer electrodes in solid-state metal-ion batteries: An in-depth review on recent advances, challenges, and future prospects. eScience Energy, 2(1), 100033. https://doi.org/10.1016/j.esen.2026.100033

Pandurangan, I., Kannadasan, M., & Balakrishnan, M. (2026). Understanding structural and electrochemical properties of metal-doped NASICON-type solid polymer electrolytes for all-solid-state sodium-metal batteries. Next Energy, 11, 100558. https://doi.org/10.1016/j.nxener.2026.100558

Pang, X., Zhang, X., Li, X., Ma, C., Wang, J., Zhang, Y., Qiao, W., Wang, J., & Ling, L. (2026). Atomic-level Nb-doped mesoporous TiO2 as multifunctional catalyst for efficient and stable Lithium-sulfur batteries. Journal of Colloid and Interface Science, 717, 140371. https://doi.org/10.1016/j.jcis.2026.140371

Patriarchi, A., Darjazi, H., Barcaioni, M., Minnetti, L., Fina, A., Filippov, A., Shah, F. U., Antzutkin, O. N., Muñoz-Márquez, M. Á., & Nobili, F. (2025). Sustainable solid-state polymer electrolyte based on PEO-Xanthan gum blend for enhanced lithium-metal batteries. Journal of Power Sources, 663, 238856. https://doi.org/10.1016/j.jpowsour.2025.238856

Pinto, R., Barbosa, J., Marijuan, A. F., Hilliou, L., Gonçalves, R., Costa, C., & Lanceros-Méndez, S. (2026). Printed solid polymer electrolytes for high-performance solid-state lithium-ion battery. Journal of Power Sources, 677, 239997. https://doi.org/10.1016/j.jpowsour.2026.239997

Rangasamy, M., Parthasarathi, S., & Wu, N. (2025). Silicon based anodes with polymer-electrolytes for solid-state lithium-ion batteries: A mini review. Journal of Energy Storage, 145, 119952. https://doi.org/10.1016/j.est.2025.119952

Ren, Y., Chen, P., Tian, K., Xiong, B., & Zhao, D. (2026). Dual-Interface engineering and solvation structure regulation enable polyether based semi-solid polymer electrolyte in high voltage lithium metal battery. Chemical Engineering Journal, 536, 175769. https://doi.org/10.1016/j.cej.2026.175769

Sabir, A., Tsai, W., Lu, S., Yu, Y., Chang, Y., & Lu, H. (2026). Fabrication and application of gel polymer electrolytes in hybrid electrolyte lithium-air batteries. Journal of the Taiwan Institute of Chemical Engineers, 106670. https://doi.org/10.1016/j.jtice.2026.106670

Shen, M., Yang, L., Liang, C., Zhang, H., Duan, C., Huang, J., Wang, P., & Ni, Y. (2025). Multiforce synergistic assembly-engineered chitosan-sodium carboxymethyl cellulose/$LiFePO_4$ composite thick electrodes toward high volumetric energy density lithium-ion batteries. Journal of Colloid and Interface Science, 701, 138706. https://doi.org/10.1016/j.jcis.2025.138706

Singh, G., & Jadoun, S. (2026). Tailoring conducting polymers for advanced electrochemical energy storage. Progress in Materials Science, 161, 101711. https://doi.org/10.1016/j.pmatsci.2026.101711

Tang, Y., Zhao, Y., & Xiang, K. (2025). Preparation and electrochemical performance of Nb-doped $LiFePO_4$/C regenerated from spent Li-ion battery cathodes. International Journal of Electrochemical Science, 21(1), 101261. https://doi.org/10.1016/j.ijoes.2025.101261

Thompson, S. W., Guimarães, T. R., Watanabe, K., Hirayama, M., & Zetterlund, P. B. (2025). Encapsulation of LiCoO2 particles with lithium containing polymer for solid state lithium-ion battery cathodes. Polymer, 324, 128255. https://doi.org/10.1016/j.polymer.2025.128255

Tu, Z., & Cao, L. (2026). Structural and electrochemical characteristics of FESN3S8@C composite anodes for Lithium-Ion batteries. International Journal of Electrochemical Science, 101396. https://doi.org/10.1016/j.ijoes.2026.101396

Wan, M., Fei, H., Liu, H., Wu, N., Passerini, S., & Bresser, D. (2025). Flame retardant polymer current collector for safer and higher energy density lithium-metal batteries. Journal of Energy Chemistry, 114, 799–807. https://doi.org/10.1016/j.jechem.2025.10.052

Wang, F., He, K., Wang, Z., Ma, H., Shi, F., Li, Z., Zhou, X., Wu, Q., Acharya, D., Doherty, C. M., Hill, M. R., Li, Z., & Wang, H. (2025). Asymmetric design of ion-transport channels in a polymeric membrane for lithium-ion sieving. Journal of Membrane Science, 738, 124807. https://doi.org/10.1016/j.memsci.2025.124807

Weckelmann, L., Lyu, H., Yang, H., Tsai, C., Dzieciol, K., Yu, S., Windmüller, A., Kungl, H., Bao, Z., & Eichel, R. (2026). A microscopic view of diffusion and failure mechanisms of lithium anodes in solid-state batteries. eScience, 100589. https://doi.org/10.1016/j.esci.2026.100589

Zeng, H., Guo, M., Poongan, A., Wang, X., Qiu, M., & Jiang, X. (2026). Design and application of $LiCoO_2$ Prelithiation material for enhanced $LiFePO_4$ cathodes in Lithium-ion batteries. Inorganic Chemistry Communications, 187, 116395. https://doi.org/10.1016/j.inoche.2026.116395

Zhang, Y., Yao, M., Tian, J., Ma, Y., & Mao, B. (2026). Surfactant-based firefighting agents: recent advances and applications in lithium-ion battery fire suppression — A critical review. Journal of Energy Storage, 165, 122347. https://doi.org/10.1016/j.est.2026.122347